

Review

# Pascoite Minerals and Potential Application of NMR Spectroscopy

Craig C. McLauchlan <sup>1,\*</sup> , Beth Trent-Ringler <sup>2</sup>  and Debbie C. Crans <sup>2,3,\*</sup> <sup>1</sup> Department of Chemistry, Illinois State University, Normal, IL 61790-4160, USA<sup>2</sup> Department of Chemistry, Colorado State University, Fort Collins, CO 80523, USA; mumbllbee@rams.colostate.edu<sup>3</sup> Cell and Molecular Biology, Colorado State University, Fort Collins, CO 80523, USA

\* Correspondence: ccmclau@ilstu.edu (C.C.M.); debbie.crans@colostate.edu (D.C.C.)

**Abstract:** The 20 minerals encompassing the pascoite family of decavanadate isopolyanion-containing  $[V_{10}O_{28}]^{6-}$  minerals include a few minerals, such as rakovanite, that have been described as containing a protonated decavanadate anion. Rakovanite was originally assigned the formula  $Na_3[H_3V_{10}O_{28}] \cdot 15H_2O$  and now is redefined with an ideal formula  $(NH_4)_3Na_3[V_{10}O_{28}] \cdot 12H_2O$ . Nuclear magnetic resonance (NMR) and particularly  $^{51}V$  NMR spectroscopy is an informative method used to describe the protonation state and speciation in both solid and solution states of materials in the chemical and life sciences. However,  $^{51}V$  NMR spectroscopy has not yet been used experimentally to distinguish the protonation state of the decavanadate ion of leaching solutions and thus contributing to the discussion regarding the controversial protonation states of decavanadate ions in gunterite, rakovanite, and nashite. In contrast, the morphology and crystal structure for apatites, vanadinite, pyromorphite, and mimetite was related to  $^{207}Pb$  NMR chemical shifts, assisting in describing the local environments of these minerals. NMR spectroscopy could be a useful method if used in the future for decavanadate-containing minerals. Currently, partial reduction of two Pascoite minerals (caseyite and nashite) is proposed and accordingly could now effectively be investigated using a different magnetic resonance technique, EPR spectroscopy.

**Keywords:** pascoite minerals; vanadium; decavanadate; NMR spectroscopy;  $^{51}V$  NMR spectroscopy solid-state; solution; speciation

**Citation:** McLauchlan, C.C.;Trent-Ringler, B.; Crans, D.C. Pascoite Minerals and Potential Application of NMR Spectroscopy. *Minerals* **2022**, *12*, 980. <https://doi.org/10.3390/min12080980>

Academic Editors: Luis

Sánchez-Muñoz and Pierre Florian

Received: 23 June 2022

Accepted: 13 July 2022

Published: 1 August 2022

**Publisher's Note:** MDPI stays neutral with regard to jurisdictional claims in published maps and institutional affiliations.



**Copyright:** © 2022 by the authors. Licensee MDPI, Basel, Switzerland. This article is an open access article distributed under the terms and conditions of the Creative Commons Attribution (CC BY) license (<https://creativecommons.org/licenses/by/4.0/>).

## 1. Introduction

Geologists, mineralogists, and chemists have characterized the solid state of over 4600 known minerals for more than a century, each using the language and lines of investigations of the respective fields [1–4]. A mineral is typically described as a naturally occurring inorganic element or compound having an orderly internal structure and characteristic chemical composition, crystal form, and physical properties [5]. With recent advances in material science and new approaches for the characterization of minerals and related synthetic compounds, characterization of their microenvironments has been explored [6]. In the case of the pascoite family of minerals, the base structure [7,8], decavanadate,  $[V_{10}O_{28}]^{6-}$  (abbreviated  $V_{10}$ ), contains a distinct anion containing 10 vanadium in oxidation state 5+ (V(V)) atoms and 28 oxygen (O) atoms flanking the V atoms, resulting in a compact structure with the dimensions  $\sim 8.3 \text{ \AA} \times 7.7 \text{ \AA} \times 5.4 \text{ \AA}$  and 3 different V atoms as shown in Figure 1a [5,9–17]. The three different V atoms in the distinct  $V_{10}$  anion,  $V_A$ ,  $V_B$ , and  $V_C$  (Figure 1) reflect the different properties of the octahedral non-oxido V and the two types of V=O atoms and support the stability that this anion has compared to the other labile, colorless oxidovanadates [18–21]. Minerals containing  $V_{10}$  will, upon dissolution, result in the intact discrete  $V_{10}$  anions.  $V_{10}$  is known to have biological activities and is extremely well studied as inhibiting enzymes such as ribonuclease, diphosphokinase,

and alkaline phosphatase; inhibit cellular growth; and have antioxidant and antidiabetic properties [9,19,22–27]. When  $V_{10}$  anions hydrolyze, they form different species, and these systems are also known to have biological activities. Studies of the biological activities and the speciation of the  $V_{10}$  will briefly be described here [19,22,23,26,28–30] since some of the pascoite minerals leach upon weathering [18].

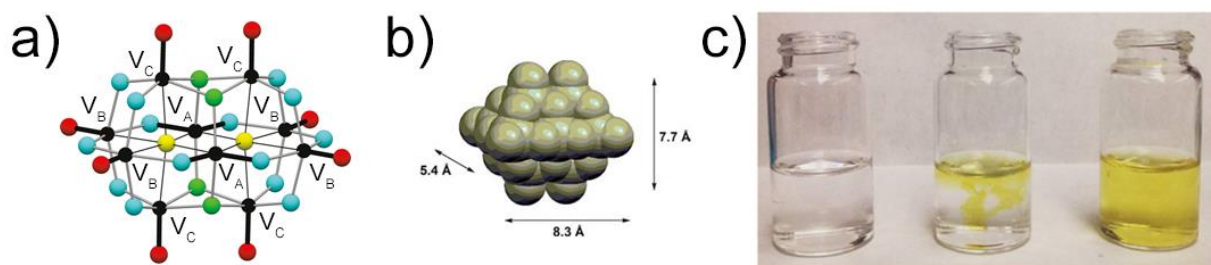


**Figure 1.** Illustration of the structure of  $V_{10}$  ion  $V_{10}O_{28}^{6-}$  (abbreviated  $V_{10}$ ): (a) schematic drawing showing the three different types of octahedral V atoms (black circles), non-oxido  $V_A$ , and two different surface active  $V_B$  and  $V_C$  atoms; [1]-coordinated O atoms = red circles, [2]-coordinated O atoms = blue circles, [3]-coordinated O atoms = green circles, [6]-coordinated O atoms = yellow circles,  $V-O_{\text{vanadyl}}$  bonds = thick black line,  $V-O_{\text{trans}}$  bonds = thin black line,  $V-O_{\text{equatorial}}$  bonds = grey shaded line; (b) space-filling diagram of a typical  $V_{10}$  anion and (c) three vials from left containing colorless oxidovanadates, colorless oxidovanadate solution with a drop of acid added forming yellow  $V_{10}$  and yellow  $V_{10}$  solution. Images used were obtained with permission from (a) Ref. [28] © 2019 by the Mineralogical Association of Canada, (b) Ref. [29] © 2014 by the World Scientific Publishing, and (c) Ref. [30] © 2022 by Elsevier.

The structural descriptions of the elemental composition of the Pascoite minerals have changed over time as improved methods have been developed and employed to elucidate the true structures [1]. Combining X-ray crystallographic insights with alternative spectroscopic and analytical methods confirms the nature of the solid state of the minerals and if they leach out upon weathering. Important chemical tools such as nuclear magnetic resonance (NMR) spectroscopy are able to characterize both what exists in the solid state and particularly what forms when these materials dissolve and leach into the environment. In the following manuscript, we will summarize studies of the Pascoite family of minerals where X-ray crystallography could be combined with spectroscopic methods to characterize not only the solid state of the minerals but also what happens when the minerals are dissolved and leached into the ground.

The geochemistry of vanadium in the environment is complex and has been well-reviewed by [1,3,4,7,18]. Knowing the properties of vanadium-containing minerals is relevant to understanding the vanadium cycle [3]. Vanadium is found in nature in a number of stable oxidation states and coordination geometries (“valences” for both/either of those terms depending on the discipline) and can easily switch between these given the microenvironment in which it is found; the main variables include the vanadium concentration, temperature, acidity (pH), reducing potential ( $E_h$ ), and oxygen concentration/pressure/fugacity. Chemists and geologists alike recognize the importance of oxygen’s presence on the oxidation state and, therefore, the coordination number and composition/speciation. Vanadium is found widely in nature, often in low concentrations in the crust despite its abundance, so large deposits of vanadium are rare [18]. One area with a higher area of vanadium concentration is in the UraVan (UraVan) mineral belt in the USA located in the southwest portion of the state of Colorado and southeast portion of the state of Utah. The blend of geochemical conditions and the industrial utility for vanadium (and uranium) of this area has led to many vanadium minerals being discovered here. In this context, the past decades have resulted in the discovery of many new vanadium minerals and often co-located minerals, with over 30 being described from this region [31].

The effects of pH and  $E_h$  on the species present can be seen by examining the Pourbaix-like diagram for vanadium minerals, as shown in Figure 2. Since the first report of vanadium minerals in the UraVan mineral belt in the 1950s, scientists have attempted to determine the reason for the higher concentration of vanadium minerals in this area [32–39]. It is widely thought that the original deposits formed by the deposition of some species on the sea floor [40] or by the reduction of vanadium by organic carbonaceous materials and  $H_2S$  at low pH and elevated ( $>80\text{ }^\circ\text{C}$ ) temperatures, resulting in deposits that include the montrosite minerals ( $V^{3+}OOH$ ) [40,41]. The vanadium(III) can readily substitute for iron(III) in minerals and is often co-located with iron-containing minerals [3]. These studies also hinted at the mobility of vanadium minerals due to being highly water soluble, especially in acidic conditions, which also often leads to oxidation. Such leaching allowed the movement of vanadium through geologic layers [40,41]. Oxidation of the reduced V(III) minerals by natural processes (e.g., weathering through oxidation by ground water or air) or human intervention (e.g., exposure to the atmosphere from mining) can lead to vanadium mobilization and the formation of so-called secondary minerals. Natural weathering and subsequent water dissolution leads to “vanadium and molybdenum being the two most abundant trace elements” in seawater [3]. Many of the  $V_{10}$  materials of interest here have been found in former mines, including all those reported since 2008 [1,42], where secondary mineralization likely occurred owing to the exposure to near surface conditions [28] as one might expect from mining activities. Indeed, mining has exposed both oxidized and more reduced phases and such minerals will often have small crystals.

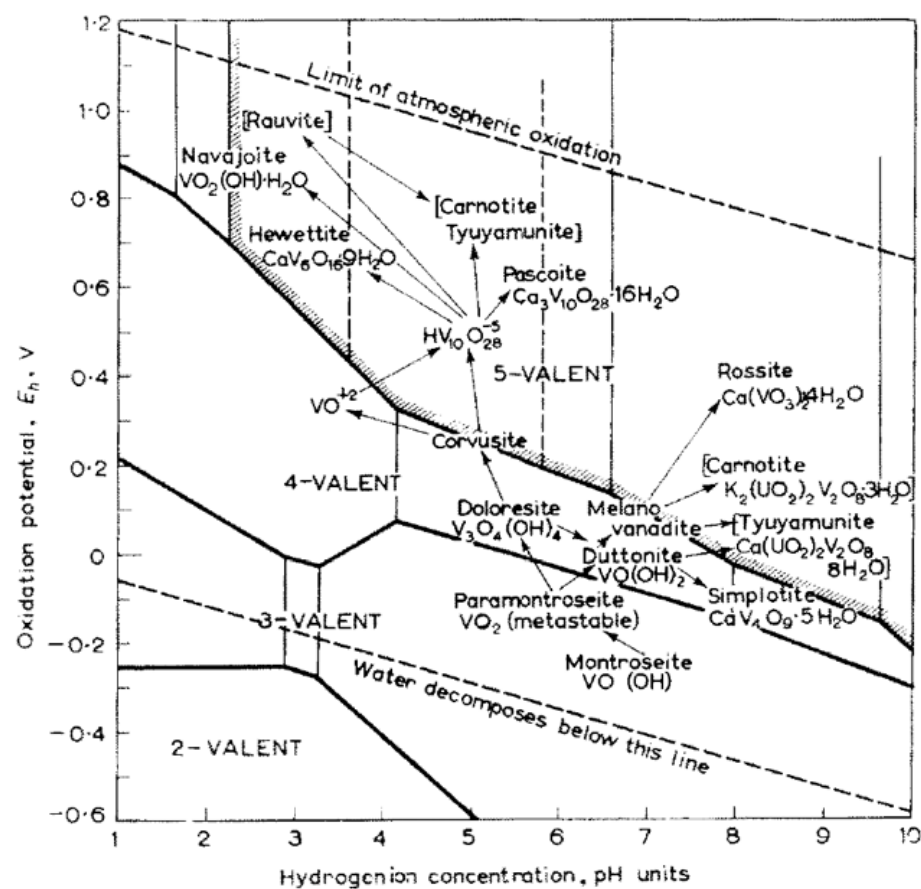


**Figure 2.** Pourbaix diagram showing oxidation potential ( $E_h$ ) vs. pH. Adapted with permission from Ref. [39]. © 1959 by Elsevier.

NMR spectroscopy is a versatile spectroscopic method that has been used for the characterization of many materials, often both in the solid state and in solution [6,43]. The

diamagnetic  $d^0$  electronic nature of the vanadium (V) ions that make up the  $V_{10}$ , coupled with largely diamagnetic cations, makes  $V_{10}$  systems more open and desirable for study [6]. The Pascoite mineral contains both V and O, both of which contain NMR active nuclei, with the V-51 (commonly written  $^{51}\text{V}$ ) isotope and the O-17 ( $^{17}\text{O}$ ) isotope, respectively, and much work has been done characterizing systems containing the  $V_{10}\text{O}_{28}$  system. Previously, we reviewed  $V_{10}$  species in the context of  $\text{Na}^+$ -containing vanadium  $V_{10}$  species [44]. Reports of various materials have been investigated in great detail and it was reported that these materials are sensitive to protonation-deprotonation in varied environments.  $^{51}\text{V}$  NMR spectroscopy is, therefore, a sensitive method for such investigations. Future applications of  $^{51}\text{V}$  NMR spectroscopy in particular in studies of pascoite and other V-containing minerals could benefit from the chemical literature and characterization of V systems.

## 2. Decavanadate ( $V_{10}$ )-Containing Minerals

Vanadium-containing minerals have been summarized in the appropriately titled review by Evans and White “The Colorful Vanadium Minerals” [4]. Since that review was first published, a number of additional vanadium-containing minerals have been discovered and described. At the time of this writing, the online database Mindat.org contained 272 minerals that include vanadium-containing minerals, although many fewer are reported elsewhere. Only a small subset of these minerals is reported to contain  $V_{10}$ . The first  $V_{10}$  mineral, pascoite, was described as early as 1914 [45], but the structures were only first reported over 50 years ago (see [33,34,37,39]) and a dramatic increase in reports has occurred since the early 2000s, as shown in Table 1 [31,32,38,46–67]. Table 1 contains the current information for 21  $V_{10}$  minerals arranged alphabetically based on name along with the chemical formula unit, several other classification systems, and first/best references. The International Mineralogical Association (IMA) Commission on New Minerals, Nomenclature and Classification (CNMNC) maintains a list of minerals, including a recent addition of a symbol [67] and the IMA Number, which is assigned in the form of the year described followed by a sequential number. The Strunz-mindat classification refers to the system originally described by the mineralogist Karl Hugo Strunz [68] and translated into English by Ernest Nickel and continued by Mindat.org. Despite there being a choice of class 08 for “vanadates” within this classification system, all classified  $V_{10}$  minerals are classified as oxides (04) and sorovanadates (HC), except for the recent definition of trebiskyite as 04.HG (unclassified oxides) [66]. With 2/3 of the minerals established within the past decade, and largely from one geographical area, there may well be other  $V_{10}$  minerals. Two previously mentioned examples include vanalite ( $\text{NaAl}_8\text{V}_{10}\text{O}_{38}\cdot 30\text{H}_2\text{O}$ ) and rauvite ( $\text{Ca}(\text{UO}_2)_2\text{V}_{10}\text{O}_{28}\cdot 16\text{H}_2\text{O}$ ), the latter having been described as early as 1922 but considered “questionable” as a mineral.

The  $V_{10}$  minerals listed in Table 1 constitute examples of structural  $V_{10}$  anions in geological microenvironments, which leads to structurally different interstitial hydrated counterions, in the parlance of Hawthorne’s structural and interstitial description model [69,70]. Because each of these minerals contains the  $V_{10}$  structural unit, they are described as the pascoite family, after the original member. Within the family, there are two groups of minerals, the pascoite group (PG) and lasalite group (LG), each containing two isostructural members [1]. These minerals in each microenvironment contain a  $V_{10}$  anion but because the counterions differ, the “speciation” varies for each of the minerals. These naturally occurring microenvironments rarely have the ideal formula and often contain solid solutions of cations. Many of these minerals have all been discovered in the same geographical region (*vide supra*). We previously summarized those reported in 2017 [44], including two protonated species. The arrangement above represents an update to previous catalogs of  $V_{10}$  minerals, including new additions and revised definitions of the fundamental unit. Specifically, two  $V_{10}$  were reported to be protonated, but these have since been corrected upon closer analysis, including some elegant updated bond-valence sums analyses and additional spectroscopy, to clarify the information obtained from X-ray diffraction studies [1,28,51]. Therefore, the structural definition and formulas of the fundamental unit have

changed over time for a couple of minerals. Although the potential speciation under the conditions the minerals formed indicates the possibility of protonation of these anions, the deprotonated  $V_{10}$  anions are now the accepted structures for gunterite and rakovinite.

**Table 1.** Pascoite family of minerals including the pascoite group (PG) and lasalite group (LG).

Mineral Species	IMA CNMNC Symbol	IMA #	Ideal Formula	Strunz-Mindat Classification	First and Best Structure Ref
Ammoniolasalite (LG)	Alas	2017-094	$(NH_4)_2Mg_2[V_{10}O_{28}] \bullet 20H_2O$	4.HC	[46]
Bluestreakite	Blu	2014-047	$K_4Mg_2[(V^{4+}_2V^{5+}_8)O_{28}] \bullet 14H_2O$	4.HC.20	[47]
Burroite	Burr	2016-079	$(NH_4)_2Ca_2[V_{10}O_{28}] \bullet 15H_2O$	4.HC.25	[48]
Caseyite *	Csy	2019-002	$[(V^{5+}_2O_2)Al_{7.5}(OH)_{15}(H_2O)_{13}]_2$ $[H_2V^{4+}V^{5+}_9O_{28}][V^{5+}_{10}O_{28}]_2 \bullet 90H_2O$	4.HC.30	[49]
Gunterite	Gun	2011-001	$Na_4Ca[V_{10}O_{28}](H_2O)_{16} \bullet 20H_2O$	4.HC.35	[50,51]
Huemulite	Hml	1965-012	$Na_4Mg[V_{10}O_{28}] \bullet 24H_2O$	4.HG.10	[38] [52]
Hughesite	Hug	2009-035a	$Na_3Al[V_{10}O_{28}] \bullet 22H_2O$	4.HC.05	[53]
Hummerite	Hum	<1959	$K_2Mg_2[V_{10}O_{28}] \bullet 16H_2O$	4.HC.10	[54,55]
Hydropascoite	Hpas	2016-032	$Ca_3[V_{10}O_{28}] \bullet 24H_2O$	4.HC.05	[56]
Kokinosite	Kkn	2013-099	$Na_2Ca_2[V_{10}O_{28}] \bullet 24H_2O$	4.HC.40	[57]
Lasalite (LG)	Las	2007-005	$Na_2Mg_2[V_{10}O_{28}] \bullet 20H_2O$	4.HC.05	[58]
Magnesiopascoite (PG)	Mpas	2007-025	$Ca_2Mg[V_{10}O_{28}] \bullet 16H_2O$	4.HC.05	[59]
Nashite	Nsh	2011-105	$Na_3Ca_2[(V^{4+}V^{5+}_9)O_{28}] \bullet 24H_2O$	4.HC.45	[60]
Okeite	Oki	2018-080	$Mg_3[V_{10}O_{28}] \bullet 28H_2O$	4.HC.50	[31]
Pascoite (PG)	Pas	<1959	$Ca_3[V_{10}O_{28}] \bullet 17H_2O$	4.HC.05	[32,55,61]
Postite	Pos	2011-060	$MgAl_2(OH)_2[V_{10}O_{28}] \bullet 27H_2O$	4.HC.55	[62]
Protocaseyite	Pcy	2020-090	$[Al_4(OH)_6(H_2O)_{12}][V_{10}O_{28}]_2 \bullet 8H_2O$	4.HC	[63]
Rakovanite	Rkv	2010-052	$(NH_4)_3Na_3[V_{10}O_{28}] \bullet 12H_2O$	4.HC.05	[64]
Schindlerite	Shi	2012-063	$(NH_4)_4Na_2[V_{10}O_{28}] \bullet 10H_2O$	4.HC.60	[57,65]
Trebiskyite	Tbk	2019-131	$Na_3Mg_2[(Ti^{4+}V_9)O_{28}] \bullet 22H_2O$	4.HG	[66]
Wernerbaurite	Wbr	2012-064	$(NH_4)_2Ca_2[V_{10}O_{28}] \bullet 16H_2O$	4.HC.25	[56,57]

\* Indicates a mineral with two formulas; # Indicate the classification IMA date.

### 3. X-ray Crystallography

Minerals were a key part of the early understanding of the structure prior to X-ray crystallography. Goniometry provided structural information well before X-ray diffraction was reported by the Braggs. The habits of crystals were known and aligned with their structure and symmetry. These early mineralogical studies were later confirmed by X-ray crystallography. The atomic arrangement of atoms in the structure lead to the macroscopic properties exhibited by the mineral species, and mineralogists performed elegant studies to determine the compositions of mineral species. X-ray diffraction relies on a repeating structure and relies on models to predict regions of electron density. The technique necessarily relies on long-range order and periodic arrangements of atoms. As such, early studies were often conducted on highly symmetric, simple structures, including minerals. The compositions were (and still are!) assumed to be idealized formula units. Techniques, X-ray flux, and sensitivity have all advanced tremendously in the past decade, but X-ray diffraction still remains a poor technique for elemental analyses. The location of hydrogen atoms in materials with and near highly electron-rich atoms remains a challenge, even with modern instrumentation. Techniques to examine the data such as bond valence sums (BVSs) remain a critical technique to deduce the correct structural models in many cases, especially those involving vanadium, oxygen, and hydrogen [69,71–77].

With the advent of improved X-ray diffraction techniques, increasingly more scientists are able to examine ever more complex structures and describe them more accurately. Weaker diffraction spots can be detected to determine longer-range order that was previously unobtainable. Scientists have been attempting to categorize the increasing complexity

of known structures [7,8], including minerals [78]. Within natural mineral systems, chemical substitution is the norm. Many examples of pure synthetic species exist, but small substitutions in solid solution produce beautiful results, e.g., corundum/sapphire/ruby. As Phillips stated in a recent review, “Minerals can only very rarely be considered pure substances, reflecting the chemical heterogeneity of natural systems, so that the crystal structure averaged over the coherent scattering length for X-rays represents an incomplete picture of the arrangement of atoms in a mineral [79]. Complete analysis of a typical major mineral in a rock will reveal a dozen or more chemical constituents present at minor-to-trace concentrations. Furthermore, most rock-forming minerals exhibit extensive formations of solid solutions, reflecting the ability of crystalline solids to accommodate ions of similar size and charge and also to compensate charge locally via coupled substitution. This chemical variability is often essential to geochemical studies that aim to deduce the formation conditions and/or subsequent pressure/temperature history of a rock [79].” Computer programs designed to help with predictions of formulae because of large uncertainties in the chemical physical analyses even exist. Despite this chemical complexity, mineral formulae are often reported in idealized forms, including those in Table 1 [31,32,38,46–67].

The  $V_{10}$ s of the pascoite family and pascoite itself offer a useful example of just such an insight into the strengths and limitations of X-ray crystallography. Pascoite was first described in 1914 as  $Ca_2V_6O_{17} \cdot 11H_2O$  from the Pasco region in Peru [45]. The atomic structure was not known at that time, but using standard mineralogical techniques such as hardness, streak, specific gravity, and birefringence, the material was gradually characterized. Furthermore, the hydration was determined through drying and gravimetric analysis, and chemical analysis was used to determine the mole ratios. The very tiny crystals were examined using goniometry and a unit cell was proposed. Later, density studies by Evans along with some crystallographic studies in 1955 led to the determination of the unit cell on artificially produced versions. It was not until 1966 that Evans published the structure of the  $V_{10}$  [34], which was subsequently corrected later that year by Swallow et al. to determine the correct waters of hydration [32]. Since that time, over 200 solid-state X-ray structures containing the discrete  $V_{10}$  anions, such as that shown in Figure 1, have been reported. Most of the diffraction studies carried out to determine the structure have been conducted on pure synthetic materials, which generally are more homogeneous and have ideal compositions compared to minerals that often contain variable microenvironments and a range of compositions [5,9–17,80]. The reported structures include  $V_{10}$  structures associated with a range of different cations [19,44] and both with and without direct bonding to other  $V_{10}$  anions as previously categorized in [75].

In addition to the many applications of X-ray crystallography for the characterization of minerals, more recently, NMR spectroscopy has been used for the characterization of several minerals after its development in the 1940s. We refer interested readers to [81]. These two methods, X-ray crystallography and NMR spectroscopy, give complementary data because X-ray diffraction studies rely on long-range order, whereas NMR spectroscopy can be much more useful for short-range order [6] as described below.

#### 4. NMR Spectroscopy

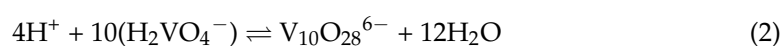
NMR spectroscopy is a versatile method that has been used for the characterization of many materials both in the solid state [81–89] and in solution [9,30,44,81,87,90–93], including minerals [2]. Materials that contain NMR-active nuclei, which occur when an element contains an isotope, which has a nonzero nuclear spin, that is an odd number of protons and/or neutrons are able to be probed with NMR spectroscopy. The most common nuclei investigated using NMR spectroscopy are hydrogen ( $^1H$ ), carbon ( $^{13}C$ ), and phosphorus ( $^{31}P$ ) [93]. These nuclei have spin  $\frac{1}{2}$ . The pascoite minerals contain V and O, and both have NMR active nuclei, with the  $^{51}V$  isotope and the  $^{17}O$  isotope. However, the nuclear spin, the natural abundance of the isotope, and the frequency for the  $^{51}V$  nucleus and the  $^{17}O$  nucleus are important for determining whether the nucleus is convenient to monitor [84,89,91–93].

$^{51}\text{V}$  and  $^{17}\text{O}$  have spins  $> \frac{1}{2}$ , with the former being  $7/2$  and the latter  $5/2$ , making both these nuclei quadrupolar with shortened relaxation times and broader signal widths [93]. The convenience of the application of these nuclei is dependent on the nuclear parameters such as the quadrupolar moment. In the case of the  $^{51}\text{V}$  nucleus, the quadrupole moment is  $0.3 \times 10^{-28} \text{ m}^2$ , placing it in the medium quadrupolar category ( $0.1 \leq Q < 1.0$ ), where signal widths are sensitive to electric field gradients but excessive linewidths are not problematic. The  $^{51}\text{V}$  has a favorable gyromagnetic ratio and the frequency of observation for  $^{51}\text{V}$  is 26.294 MHz near  $^{13}\text{C}$  (25.145 MHz) at a field of 2.35 T and it is a very convenient nuclei to observe [93]. In contrast, the calculated receptibility of the  $^{17}\text{O}$  nucleus is  $10^{-5}$  of that of the  $^1\text{H}$ , it has a quadrupolar moment of  $-2.6 \times 10^{-2}$  barn, it has a low gyromagnetic ratio, and the frequency for  $^{17}\text{O}$  is 13.557 MHz, which makes this nucleus a much greater challenge spectroscopically. These facts, combined with  $^{51}\text{V}$  being 99.76% abundant and  $^{17}\text{O}$  being 0.0037% abundant, mean that  $^{51}\text{V}$  is much easier to observe. The abundance of the isotope is important for the size of the signal and can be counteracted by using enriched samples; however, such spectral characterization is more complicated if, for example, enriched water ( $\text{H}_2^{17}\text{O}$ ) is used because of the many exchange reactions that can occur. Regardless, studies have been carried out demonstrating that such challenges can be overcome [93].

In the following, we will show some NMR spectroscopic applications of the  $^{51}\text{V}$  nucleus and since some of these minerals are water soluble, we will discuss both solution and solid-state applications of  $^{51}\text{V}$  NMR spectroscopy. Specifically, we will show the solution spectra of  $\text{V}_{10}$ . Since there are no solid-state  $^{51}\text{V}$  NMR studies of pascoite minerals, we will show the spectra of vesignieite,  $\text{BaCu}_3\text{V}_2\text{O}_8(\text{O})_2$  where some spectra have been recorded. However, we advocate for applications of  $^{51}\text{V}$  in the future for studies of pascoite minerals and the mineral leaching solutions.

## 5. Speciation

IUPAC recommend that the term “speciation” is used to indicate the distribution of species in a sample and used to describe the “species distribution” [94]. The importance of determining what forms of compounds are present has become increasingly important since it is generally recognized that different forms of a material can cause different responses and reactivities in many different fields [22,23,26,90,94–100]. Methods have been and continue to be developed to characterize different species [101]. The term speciation is often used by solution chemists to describe the species that form in aqueous solution with defined stoichiometry (p,q) as shown in Equation (1) [20,21,99,102,103]. Equation (2) shows  $\text{H}^+$  and vanadate (more properly dihydrogenorthovanadate,  $\text{H}_2\text{VO}_4^-$ ) forming  $\text{V}_{10}$ , a complex with the stoichiometry defined by  $p = 4$  and  $q = 10$  in an equilibrium reaction. Speciation studies will result in a series of constants that represent the system and allow for the prediction of the species distribution in aqueous solution under these equilibrium conditions [18,20,21,99,100,103,104]:



In the case of  $\text{V}_{10}$ , the formation is favored in acidic solution as shown in Equation (2). The formation of the orange  $\text{V}_{10}$  from colorless oxidovanadate solutions is a signature reaction documenting the conversion from the colorless monomeric white crystalline orthovanadate, a simple phosphate analog, to the compact orange  $\text{V}_{10}$  structure, as shown in Figure 1 [19,23]. The color of the compact anionic structure can change as the counter ion changes, but for most minerals, it is responsible for the orange color, as shown in Figure 1c. However, as the pH of the solution increases, the stability of  $\text{V}_{10}$  generally decreases. At neutral pH, the half-life of  $\text{V}_{10}$  ranges from 10 to about 72 h depending on the other solution components and temperature, whereas in basic solution, the lifetime is reduced to a few hours or less [19]. At pH values around 5–6, as obtained in aqueous

solutions saturated with  $\text{CO}_2/\text{H}_2\text{CO}_3$ , the  $\text{V}_{10}$  anion is stable, which is likely to be the case for solutions obtained when water is leaching through soils.

## 6. $^{51}\text{V}$ NMR Spectroscopy of $\text{V}_{10}$ in Aqueous Solution and pH Variation in the Chemical Shift

$^{51}\text{V}$  NMR spectroscopy is a convenient method for determining the speciation of the V(V) in aqueous solution. Depending on the pH range, these studies can be non-trivial because speciation studies require that the reactions are at equilibrium. Some V(V) species, such as the smaller colorless oxidovanadates in their various protonation states of  $\text{VO}_4^{3-}$  ( $\text{V}_1$ ),  $\text{V}_2\text{O}_7^{4-}$  ( $\text{V}_2$ ),  $\text{V}_4\text{O}_{12}^{4-}$  ( $\text{V}_4$ ), and  $\text{V}_5\text{O}_{15}^{5-}$  ( $\text{V}_5$ ), rapidly equilibrate, whereas the orange  $\text{V}_{10}$  species equilibrates slowly at neutral and basic pH values. However, the early work characterizing the  $\text{V}_{10}$  structurally by Evans via X-ray crystallography [34] was complemented by the speciation studies of the Petterson group defining the species present in solution under various conditions [20,21]. The  $\text{V}_{10}$  anion has three different V atoms:  $\text{V}_A$ ,  $\text{V}_B$ , and  $\text{V}_C$  (Figure 1a), that have different  $^{51}\text{V}$  NMR signals in a ratio of 1:2:2. The two octahedral internal non-oxo vanadium atoms shown as  $\text{V}_A$  in Figure 1a are observed as a broad signal furthest downfield at  $-425$  ppm. One octahedral V-oxo signal is observed at  $-498$  ppm for the V atoms on the short side of the  $\text{V}_{10}$  structure ( $\text{V}_B$ ) and the other at  $-525$  ppm for the V atoms on the long side of the  $\text{V}_{10}$  structure ( $\text{V}_C$ ), demonstrating the effects of the oxido-group and the specific geometry on the chemical shift of the V signal. In Figure 3, a speciation diagram of the V(V) species in solution is shown for a system at 50 mM  $\text{NaVO}_3$  and 50 mM V atoms (and 5 mM  $\text{V}_{10}$ ) [30]. The best experimental data for the calculation of the formation constants are obtained using more than one experimental method, including  $^{51}\text{V}$  NMR spectroscopy, as was pioneered by the Petterson and Howard groups [20,21,92]. Once formation constants are available, calculations can be carried out using programs such as *HYSS* as described in [26].

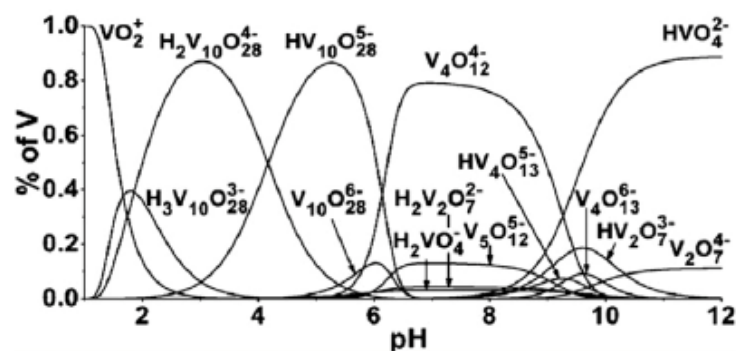


**Figure 3.** Distribution diagram in a solution of 50 mM  $\text{NaVO}_3$  and 50 mM V atoms (5 mM  $\text{V}_{10}$ ) in 0.15 M NaCl as a function of pH. The species are indicated by their formulas, including showing different protonation states. The figure is adapted with permission Ref. [90]. © 2012 by the American Chemical Society.

NMR chemical shifts are known to vary with the protonation states and can be used for titration of the protonation/deprotonation of the  $\text{V}_{10}$  and to determine the respective  $\text{pK}_a$  values [20,21,92]. To illustrate the sensitivity of the  $^{51}\text{V}$  NMR chemical shift to pH, we recorded the  $^{51}\text{V}$  NMR spectra of 5 mM  $\text{V}_{10}$  (50 mM metavanadate) from pH 2.96 to 7, which covered the pH range of the final  $\text{pK}_a$  values for  $\text{V}_{10}$  [30]. The  $^{51}\text{V}$  NMR spectra are shown in Figure 4a. The  $^{51}\text{V}$  chemical shift of the  $\text{V}_B$  and  $\text{V}_C$  signals varied, showing a distinct pH dependence consistent with deprotonation as the pH increased. In contrast, the  $\text{V}_A$  signals changed much less consistently, with the  $\text{V}_A$  atom being located internally in the  $\text{V}_{10}$  anion and thus being much less sensitive to the change in the protonation state. These data show that the protonation state affects the chemical shift and in Figure 4b, the chemical shifts for  $\text{V}_A$ ,  $\text{V}_B$ , and  $\text{V}_C$  are plotted as a function of pH. The pH titration curves are readily observed, giving rise to data allowing the calculation of the  $\text{pK}_a$  values for the

protonation of the  $V_{10}$  anion. Each of the V atoms give rise to a  $pK_a$  value, and they were 4.8 for both  $V_B$  and  $V_C$ , showing a slight difference depending on the location of the V atom in the  $V_{10}$  anion. These values are similar to those reported previously of 5.5 to 6.0 for the deprotonation of monoprotinated  $V_{10}$  ( $HV_{10}O_{28}^{5-}$ ) [30]. These data illustrate that the protonation state of the  $V_{10}$  anion can clearly be observed using the chemical shifts of the  $V_{10}$  anion. This concept has already been used to characterize the protonation state of the  $V_{10}$  species that is observed in reverse micelles [105]. Figure 4a also demonstrates the importance of pH in the stability of  $V_{10}$ , as rising basicity impacts the equilibrium shown in Equation (2), leading to other polyoxidovanadates.

These studies demonstrate how the  $^{51}V$  NMR spectra of  $V_{10}$  solutions characterize the species that leach from the mineral deposits. Although the amount of vanadium in such leaching solution will be very low,  $^{51}V$  NMR spectroscopy is very sensitive due to the high natural abundance of V and the quadrupolar nucleus, which allows for rapid accumulation of scans, resulting in spectra with high signal to noise. However, solution studies require the dissolution of the minerals, and, hence, it is of interest to attempt non-destructive solid-state NMR spectroscopy of these systems as well.

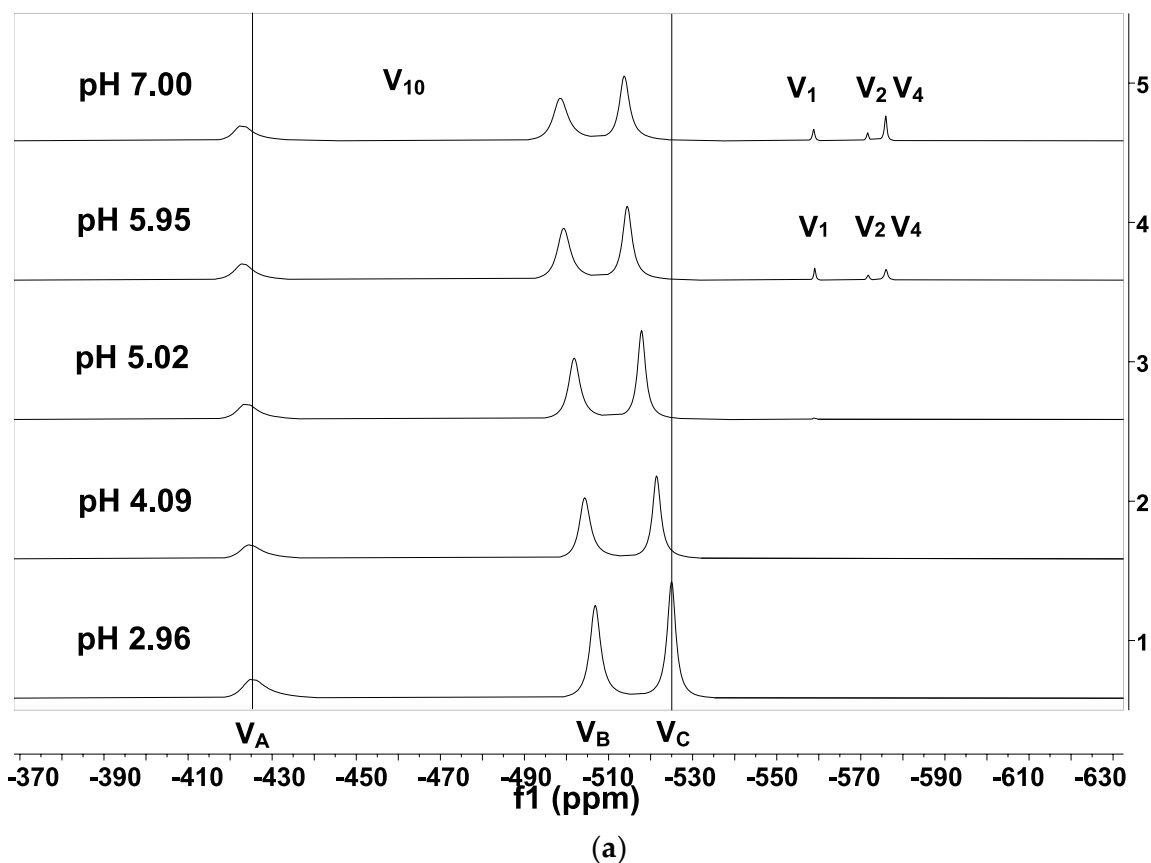
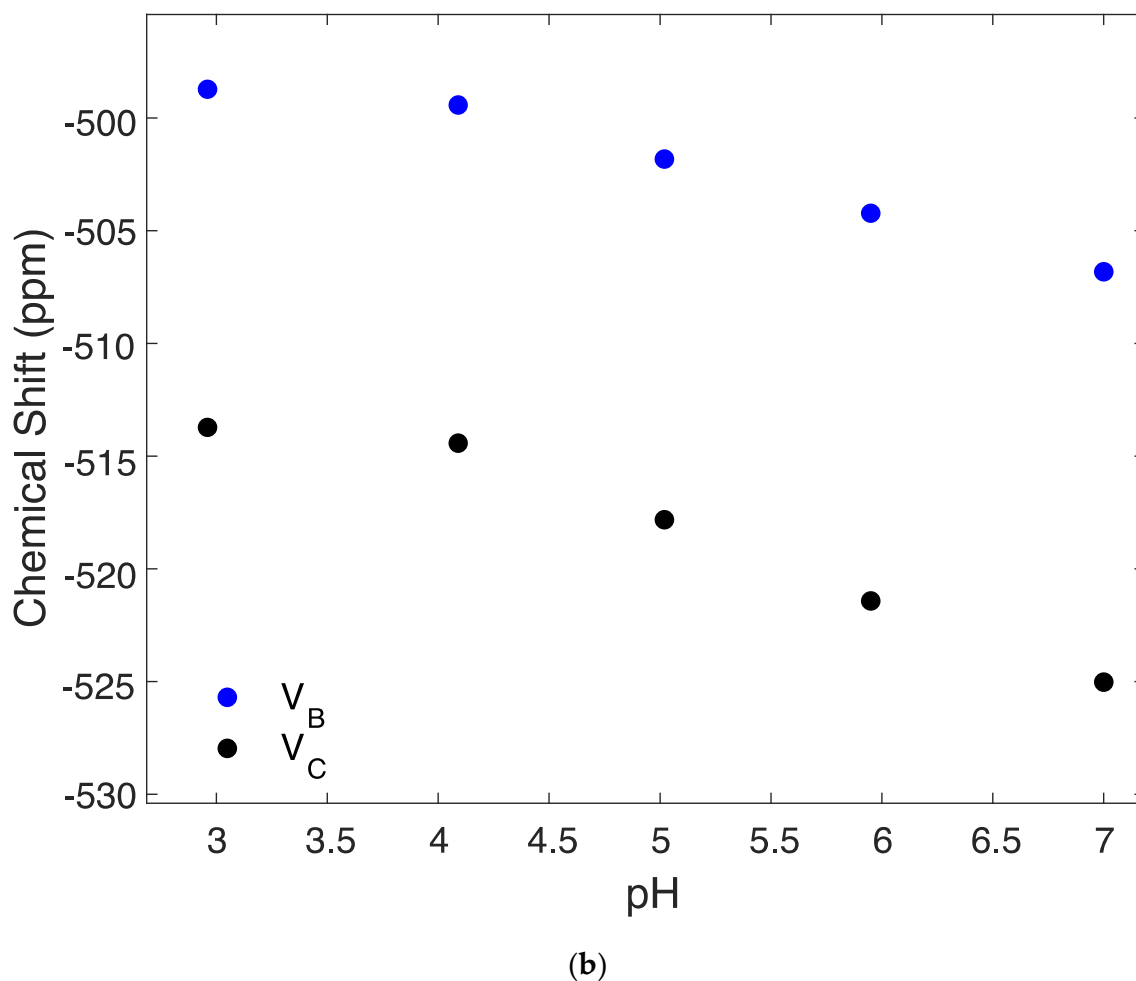


Figure 4. Cont.



**Figure 4.** The  $^{51}\text{V}$  NMR spectra of a solution of 5 mM vanadate (and 0.5 mM  $\text{V}_{10}$ ) is shown from pH 2.96 to 7.00; assignments are  $V_A$  (−414 ppm),  $V_B$  (−498 ppm), and  $V_C$  (−525 ppm) (a); plots of the chemical shift as a function of pH for the three different V atoms in the  $\text{V}_{10}$  anion, of the two  $^{51}\text{V}$  nuclei on the surface of the anion,  $V_B$  (−498 ppm), and  $V_C$  (−525 ppm) (b). See Figure 1 caption and the text for the abbreviations.

## 7. Solid-State NMR Spectroscopy

The application of  $^{51}\text{V}$  NMR to study solid vanadium-containing complexes of fundamental, technological, and biological relevance has grown rapidly in recent years [106] due to the ability to acquire high-quality magic angle spinning spectra of both the central and satellite NMR transitions of the  $^{51}\text{V}$  nucleus ( $I = 7/2$ ). Studies have demonstrated that the quadrupolar coupling, the chemical shift anisotropy (CSA), and the electric field gradient (EFG) tensors can be determined from the solid-state NMR spectra. Since these parameters are sensitive to the local vanadium environment, they can be used to understand changes in the local molecular orbital structure and ground state charge distribution of the vanadium [82,107]. Solid-state  $^{51}\text{V}$  NMR has been useful for the study of the electronic properties of  $^{51}\text{V}$ -containing inorganic compounds [82,83,85,87,88,108–114] and vanadium-containing protein complexes [86,115]. An important link between the parameters measured using solid-state  $^{51}\text{V}$  NMR and the molecular structure of the vanadium atom is obtained using DFT calculations [86,87,115–120].

Solid-state NMR spectroscopy has been used to investigate the local environment of the Al and Si distribution in aluminosilicate minerals, where the major component is crystalline oxides and silicates [6]. Minerals containing crystalline silicides and oxides are among the three most common elements in Earth's crust, and together account for

over 90% of its volume [6,81]. NMR spectroscopic studies measured chemical shifts and quadrupolar coupling parameters, and identified interactions between adjacent cations and anions, bond lengths, bond angles, and the symmetry of the systems [6,81]. In this manner, NMR spectroscopy was able to shed light on many long-standing problems in the structure and composition of unsolved mineral systems. Specifically, XRD methods were found to result in weak or similar scattering factors, imperfect (impure) sample concentrations that were too low to affect cell parameters, short-range order effects, and disorder effects at distances shorter than expected for coherent X-ray scattering.

Materials containing little or negligible amounts of paramagnetic ions with unpaired electron spins are the most studied because they minimize any potential effects of electron–nuclear spin couplings [6,121]. In solution, paramagnetic effects are relatively well known and, in fact, shift reagents (also referred to as contrast agents) containing unpaired electron spins are routinely used to increase the frequency range or increase spin relaxation in the solution-state NMR and magnetic resonance imaging (abbreviated MRI) [113,122,123]. Less information is available about the paramagnetic effects by solid-state NMR and NMR line-broadening effects can be very large. However, since the ranges in the chemical shifts for paramagnetic peaks are generally much larger than normal chemical shifts, there could be an enhanced sensitivity to small structural variations, and it has been suggested that pseudocontact shift and the Fermi contact shift may be detectable when the sample is subjected to an MAS experiment [123].

Some studies have been reported with vanadium-substituted minerals. Vanadium has a diverse coordination chemistry and can be routinely found in environments with coordination numbers ranging from three to eight, giving rise to many complexes that have useful chemical and biochemical properties [89,104]. In contrast to the pascoite family of minerals that contain  $V_{10}$  as a discrete anion, in all of which vanadium is in a six-coordinate octahedral coordination environment for every member of the family, in vanadium-substituted minerals, there is greater variety in the coordination geometries.  $V^{3+}$ -substituted tourmalines were investigated; however, no NMR spectroscopy techniques were used to characterize the materials [124–126]. In flux-grown  $Y_{1-x}M_xPO_4$ ,  $M=V$ , with a random cation distribution with a variable oxidation state of the V. The authors were able to use  $^{31}P$  chemical shifts to characterize the environments of both the P and V atoms [43].  $^{51}V$  NMR was successfully used to study V oxides on  $SiO_2$  [127]. Solid-state MAS  $^{51}V$  NMR spectroscopy was used to investigate the supported  $V_2O_5/SiO_2$  catalysts to investigate the coordination of the vanadium oxide as a function of the environmental conditions [128]. The spectra indicate a signal for a single dehydrated surface vanadium oxide species at  $-675$  ppm and two signals for vanadium oxide species at  $-566$  and  $-610$  ppm [128]. Studies of  $Pb_xCa_{10-x}(VO_4)_y(PO_4)_{6-y}(OH)_2$  using lead and vanadium replacement of the hydroxyapatite mineral were monitored by  $^{31}P$ ,  $^{43}Ca$ ,  $^{207}Pb$ ,  $^{51}V$ , and  $^1H$  NMR spectroscopy. The impact of lead insertion in this material was visible using both solid-state  $^{51}V$  and  $^{207}Pb$  NMR spectroscopy [129]. Accordingly, the morphology and crystal structure for apatites, vanadinite, pyromorphite, and mimetite can be related to  $^{207}Pb$  and the  $^{51}V$  NMR chemical shifts and assist in describing the local environments of the Pb cation in these substituted minerals. In addition, the use of  $^1H$  NMR spectroscopy to examine vanadium silicates (including the minerals cavansite, pentagonite, and haradaite) to determine the mineral hydration level was introduced [130]. To the best of our knowledge, there is only one mineral that has been studied by solid-state  $^{51}V$  NMR, the kagome antiferromagnet vesignieite,  $BaCu_3V_2O_8(OH)_2$  [131,132]. Quilliam et al. [131] and Yoshida et al. [132] both examined NMR line shifts to examine the magnetic susceptibility (Figure 5) with varying field strength, frequency, and temperature.

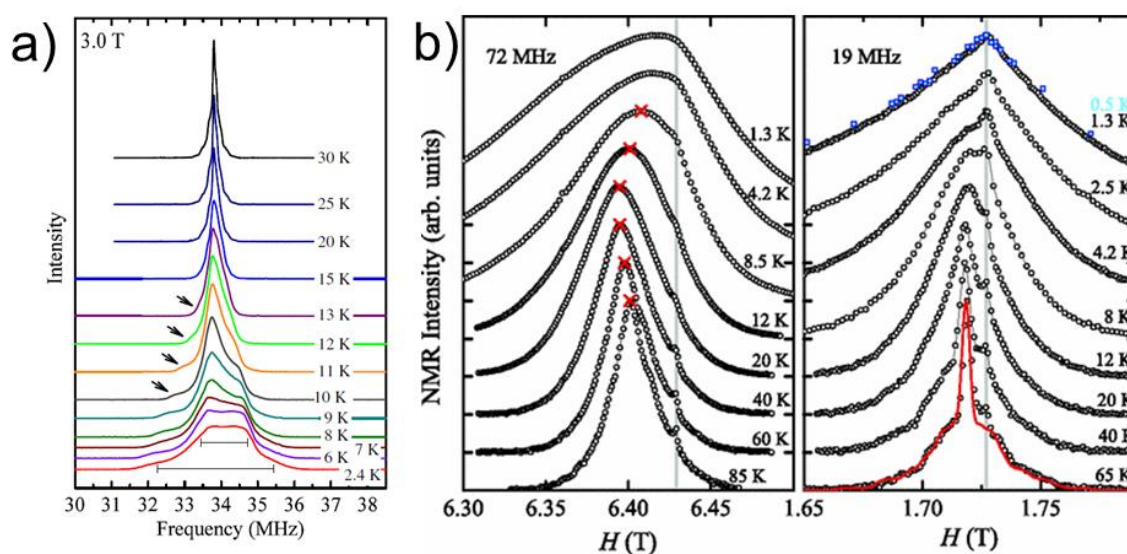


**Figure 5.** The  $^{51}\text{V}$  NMR spectra of vesignieite,  $\text{BaCu}_3\text{V}_2\text{O}_8(\text{O})_2$ . (a) Fixed magnetic field  $B = 3.0\text{ T}$  with varying temperature. Reproduced with permission from [132]. © 2013 The Physical Society of Japan. (b) Spectra from 72 (left) and 19 MHz (right) normalized for visibility. Gray lines indicate the reference field, the red line is powder simulation for comparison. Red 'x's determine the line shift. Figure reprinted with permission from Ref. [131]. © 2011 by the American Physical Society.

None of these studies observed  $\text{V}_{10}$  using solid-state  $^{51}\text{V}$  NMR spectroscopy for members of the Pascoite family. The presence of hydrated  $\text{V}_{10}$  clusters in vanadia gels and deprotonated species was anticipated but not observed [87]. However, a study following the polymerization of the  $\text{V}_2\text{O}_5$  gels led to the observation of  $\text{V}_{10}$  protonation and hydrolysis [133].

## 8. Vanadium V(IV) in $\text{V}_{10}$ Systems

Although  $\text{V}_{10}$  generally contains V(V), reports have been made showing that when subjected to the right treatment, some portion of the V atoms in the molecule can have their oxidation state reduced, presumably to V(IV). Although some of these  $\text{V}_{10}$  derivatives have been stabilized by supporting ligands, it has recently been reported that anionic  $\text{V}_{10}$  could be reduced [134]. In  $\text{V}_{10}$  systems, such reduction is often visibly noticeable by the presence of a blue or green species in lieu of the typical orange color, e.g., in bluestreakite [47]. These multivalence polyoxidometalates can be a challenge, and can also be characterized using additional spectroscopic methods such as electron paramagnetic resonance (EPR). In the case of  $\text{V}^{\text{V}}\text{V}^{\text{IV}}$  multivalence polyoxidometalates, the presence of the V(IV) atoms and unpaired electrons complicates the use of  $^{51}\text{V}$  NMR spectroscopy because to record NMR spectra, the unpaired electrons must be paired, and that may not be possible in such rigid structures [135].

Should NMR alone prove impossible or impractical owing to the paramagnetic V(IV), then, these compounds are, therefore, investigated using a combination of EPR and NMR spectroscopy to characterize the solutions. With this combination of methods, the  $\text{V}_{10}$  protonation and reduction can be monitored, for example, as has been seen with solutions of sodium metavanadate [133]. For example, the characterization of  $\text{V}_{\text{ox}}$  from  $\text{V}_2\text{O}_5$  deposited on  $\text{TiO}_2$  was investigated by  $^{51}\text{V}$  MAS NMR spectroscopy and EPR spectroscopy. The spectra show that the reaction kinetics and the consumption of  $\text{V}(\text{V})\text{O}_2^+$  obtained from  $\text{V}_{10}$  will form vanadate polymeric species in solution with an environment similar to that of the dioxidovanadium cation [133]. Indeed, as described above, a solid-state NMR study following the polymerization of the  $\text{V}_2\text{O}_5$  gels led to the observation of  $\text{V}_{10}$  protonation and hydrolysis [128].

## 9. Conclusions and Future Applications

NMR spectroscopy is an informative method used to describe the protonation state and speciation in both solid and solution states of materials in the chemical and life sciences.  $^{51}\text{V}$  NMR spectroscopy would be particularly useful for the characterization of many vanadium-containing minerals, especially those including the pascoite family of minerals containing  $\text{V}_{10}$ . Although dissolution may cause some change in speciation, so far, the solid-state  $^{51}\text{V}$  NMR spectra of  $\text{V}_{10}$  materials have not been used to investigate these materials although some reports of substituted minerals have been investigated by solid-state  $^{51}\text{V}$  NMR spectroscopy. One reason these studies have not yet been done is because these vanadium minerals are rare and often found in small quantities, and the 30–50 mg of pure mineral needed may not be accessible (although the required quantities are decreasing as techniques and rotors improve). In addition, many of these minerals are soluble and interference from the paramagnetic cations present in a complex natural mineral solution is possible.

EPR could also be beneficial for the investigation of  $\text{V}_{10}$  species because partial reduction of some of the vanadium atoms in oxidation state +5 reduce to oxidation state +4 within the mineral has recently been shown to take place for at least two of the known minerals shown in Table 1. Because EPR is more sensitive than NMR, smaller quantities of materials are needed, and solid-state EPR (low temperature measurements) would make the technique non-destructive. EPR spectroscopy will also bolster the mixed V(IV)/V(V) assignment in these minerals. Importantly, however, the  $^{51}\text{V}$  NMR (and/or  $^1\text{H}$  NMR) spectra of  $\text{V}_{10}$  are sensitive to the protonation state, so the  $^{51}\text{V}$  NMR spectra could add additional proof to reassignment of the protonation state of the  $\text{V}_{10}$  anion. NMR spectroscopy is a valuable future technique, and we encourage spectroscopists to study these complex minerals and mineralogists to venture and work with this new technique.

**Author Contributions:** Conceptualization, D.C.C. and C.C.M.; writing—original draft preparation, C.C.M. and D.C.C.; writing—review and editing, C.C.M., B.T.-R. and D.C.C. All authors have read and agreed to the published version of the manuscript.

**Funding:** This research was funded by Illinois State University to C.C.M. and from Colorado State University to D.C.C.

**Informed Consent Statement:** Not applicable.

**Data Availability Statement:** Not applicable.

**Acknowledgments:** We thank Heide A. Murakami for technical assistance in preparing this manuscript. The suggestions and comments of the anonymous reviewers were also helpful.

**Conflicts of Interest:** The authors declare no conflict of interest.

## References

1. Kampf, A.R.; Hughes, J.M.; Cooper, M.A.; Hawthorne, F.C.; Nash, B.P.; Olds, T.A.; Adams, P.M.; Marty, J. The Pascoite Family of Minerals, Including the Redefinition of Rakovanite. *Can. Mineral.* **2021**, *59*, 771–779. [[CrossRef](#)]
2. Ashbrook, S.E.; Dawson, D.M. NMR spectroscopy of minerals and allied materials. *Nucl. Magn. Reson.* **2016**, *45*, 1–52. [[CrossRef](#)]
3. Huang, J.H.; Huang, F.; Evans, L.; Glasauer, S. Vanadium: Global (bio)geochemistry. *Chem. Geol.* **2015**, *417*, 68–89. [[CrossRef](#)]
4. White, J.S.E.; Evans, H.T. The Colorful Vanadium Minerals: A Brief Review and a New Classification. *Mineral. Rec.* **1987**, *18*, 333–340.
5. Kaziev, G.Z.; Oreshkina, A.V.; Quinones, S.H.; Stepnova, A.F.; Zavodnik, V.E.; de Ita, A.; Alekseev, D.A. Synthesis and crystal structure of sodium isopolyvanadate  $[\text{Na}_2(\text{H}_2\text{O})_8]_2\text{H}_2[\text{V}_{10}\text{O}_{28}] \cdot 4\text{H}_2\text{O}$ . *Russ. J. Coord. Chem.* **2010**, *36*, 887–890. [[CrossRef](#)]
6. Stebbins, J.F.; McCarty, R.J.; Palke, A.C. Solid-state NMR and short-range order in crystalline oxides and silicates: A new tool in paramagnetic resonances. *Acta Crystallogr. C* **2017**, *73*, 128–136. [[CrossRef](#)]
7. Krivovichev, S.V. Polyoxometalate clusters in minerals: Review and complexity analysis. *Acta Crystallogr. B* **2020**, *76*, 618–629. [[CrossRef](#)]
8. Krivovichev, S.V. Which Inorganic Structures are the Most Complex? *Angew. Chem. Int. Ed.* **2014**, *53*, 654–661. [[CrossRef](#)]
9. Turner, T.L.; Nguyen, V.H.; McLauchlan, C.C.; Dymon, Z.; Dorsey, B.M.; Hooker, J.D.; Jones, M.A. Inhibitory effects of decavanadate on several enzymes and *Leishmania tarentolae* In Vitro. *J. Inorg. Biochem.* **2012**, *108*, 96–104. [[CrossRef](#)]
10. Fratzky, D.; Schneider, M.T.; Rabe, S.; Meisel, M.  $(\text{NH}_4)_4\text{Na}_2[\text{V}_{10}\text{O}_{28}] \cdot 10\text{H}_2\text{O}$ . *Acta Crystallogr. C* **2000**, *56*, 740–741. [[CrossRef](#)]

11. Guo, H.-X.; Yao, Z.-L.  $\text{Na}_6(\text{H}_2\text{O})_{20}(\text{V}_{10}\text{O}_{28})\cdot 4\text{H}_2\text{O}$ , a novel polyvanadate(V) with a three-dimensional framework. *Acta Crystallogr. C* **2007**, *63*, i51–i53. [[CrossRef](#)]
12. Ksiksi, R.; Graia, M.; Jouini, T. Sel mixte de lithium et de sodium eicosahydrate,  $\text{Na}_{5.22}\text{Li}_{0.78}[\text{V}_{10}\text{O}_{28}]\cdot 20\text{H}_2\text{O}$ . *Acta Crystallogr. E* **2005**, *61*, i177–i179. [[CrossRef](#)]
13. Lee, U.; Joo, H.-C. A novel monoprotonated decavanadate,  $\text{K}_4\text{Na}[\text{HV}_{10}\text{O}_{28}]\cdot 10\text{H}_2\text{O}$ . *Acta Crystallogr. E* **2004**, *60*, i22–i24. [[CrossRef](#)]
14. Iida, A.; Ozeki, T.  $\text{Cu}_3\text{V}_{10}\text{O}_{28}\cdot 24\text{H}_2\text{O}$  and  $\text{CuNa}_4\text{V}_{10}\text{O}_{28}\cdot 23\text{H}_2\text{O}$ . *Acta Crystallogr. C* **2003**, *59*, i41–i44. [[CrossRef](#)]
15. Lee, U.; Joo, H.-C. Potassium–sodium double salt of decavanadate,  $\text{K}_4\text{Na}_2[\text{V}_{10}\text{O}_{28}]\cdot 10\text{H}_2\text{O}$ . *Acta Crystallogr. E* **2003**, *59*, i122–i124. [[CrossRef](#)]
16. Matias, P.M.; Pessoa, J.C.; Duarte, M.T.; Madeira, C. Tetrapotassium disodium decavanadate(V) decahydrate. *Acta Crystallogr. C* **2000**, *56*, e75–e76. [[CrossRef](#)]
17. Crans, D.C.; Mahroofatahir, M.; Anderson, O.P.; Miller, M.M. X-ray structure of  $(\text{NH}_4)_6(\text{GLY-GLY})_2\text{V}_{10}\text{O}_{28}\cdot 4\text{H}_2\text{O}$ —Model studies for polyoxometalate-protein interactions. *Inorg. Chem.* **1994**, *33*, 5586–5590. [[CrossRef](#)]
18. Gustafsson, J.P. Vanadium geochemistry in the biogeosphere -speciation, solid-solution interactions, and ecotoxicity. *Appl. Geochem.* **2019**, *102*, 1–25. [[CrossRef](#)]
19. Aureliano, M.; Crans, D.C. Decavanadate ( $\text{V}_{10}\text{O}_{28}^{6-}$ ) and oxovanadates: Oxometalates with many biological activities. *J. Inorg. Biochem.* **2009**, *103*, 536–546. [[CrossRef](#)]
20. Pettersson, L.; Hedman, B.; Anderson, I.; Ingri, N. Multicomponent polyanions. 34. Hydrolysis and equilibria of the  $\text{H}^+ - \text{H}_2\text{VO}_4^-$  system in 0.6 M Na(Cl). *Chem. Scr.* **1983**, *22*, 254–264.
21. Pettersson, L.; Hedman, B.; Nenner, A.-M.; Anderson, I. Multicomponent polyanions. 36. Hydrolysis and redox equilibria of the  $\text{H}^+ - \text{HVO}_4^{2-}$  system in 0.6 M Na(Cl). A complementary potentiometric and  $^{51}\text{V}$  NMR study at low vanadium concentrations in acid solution. *Acta Chem. Scand. A* **1985**, *39*, 499–506. [[CrossRef](#)]
22. Aureliano, M.; Gumerova, N.I.; Sciortino, G.; Garribba, E.; McLauchlan, C.C.; Rompel, A.; Crans, D.C. Polyoxidovanadates' interactions with proteins: An overview. *Coord. Chem. Rev.* **2022**, *454*, 214344. [[CrossRef](#)]
23. Aureliano, M.; Gumerova, N.I.; Sciortino, G.; Garribba, E.; Rompel, A.; Crans, D.C. Polyoxovanadates with emerging biomedical activities. *Coord. Chem. Rev.* **2021**, *447*, 214143. [[CrossRef](#)]
24. Choate, G.; Mansour, T.E. Studies on heart phosphofructokinase-decavanadate as a potent allosteric inhibitor at alkaline and acidic pH. *J. Biol. Chem.* **1979**, *254*, 1457–1462. [[CrossRef](#)]
25. Messmore, J.M.; Raines, R.T. Decavanadate inhibits catalysis by ribonuclease A. *Arch. Biochem. Biophys.* **2000**, *381*, 25–30. [[CrossRef](#)]
26. Samart, N.; Arhouma, Z.; Kumar, S.; Murakami, H.A.; Crick, D.C.; Crans, D.C. Decavanadate Inhibits Mycobacterial Growth More Potently Than Other Oxovanadates. *Front. Chem.* **2018**, *6*, 519. [[CrossRef](#)]
27. Crans, D.C. Antidiabetic, Chemical, and Physical Properties of Organic Vanadates as Presumed Transition-State Inhibitors for Phosphatases. *J. Org. Chem.* **2015**, *80*, 11899–11915. [[CrossRef](#)]
28. Cooper, M.A.; Hawthorne, F.C.; Kampf, A.R.; Hughes, J.M. Determination of  $\text{V}^{4+}:\text{V}^{5+}$  ratios in the  $[\text{V}_{10}\text{O}_{28}]^{(n-)}$  decavanadate polyanion. *Can. Mineral.* **2019**, *57*, 235–244. [[CrossRef](#)]
29. Samart, N.S.; Haller, K.J.; Aureliano, M.; Crans, D.C. Interaction of decavanadate with interfaces and biological model membrane systems: Characterization of soft oxometalate systems. *J. Mol. Eng. Mat.* **2014**, *2*, 1–21. [[CrossRef](#)]
30. Kostenkova, K.; Scalse, G.; Gambino, D.; Crans, D.C. Highlighting the roles of transition metals and speciation in chemical biology. *Curr. Opin. Chem. Biol.* **2022**, *69*, 102155. [[CrossRef](#)]
31. Kampf, A.R.; Adams, P.M.; Nash, B.P.; Marty, J.; Hughes, J.M. Okeite,  $\text{Mg}_3[\text{V}_{10}\text{O}_{28}]\cdot 28\text{H}_2\text{O}$ , a new decavanadate mineral from the Burro mine, Slick Rock Mining District, San Miguel County, Colorado, USA. *Can. Mineral.* **2020**, *58*, 125–135. [[CrossRef](#)]
32. Swallow, A.G.; Ahmed, F.R.; Barnes, W.H. Crystal Structure of Pascoite  $\text{Ca}_3\text{V}_{10}\text{O}_{28}\cdot 17\text{H}_2\text{O}$ . *Acta Crystallogr.* **1966**, *21*, 397–405. [[CrossRef](#)]
33. Evans, H.T. Crystal structure of decavanadate  $\text{K}_2\text{Zn}_2\text{V}_{10}\text{O}_{28}\cdot 16\text{H}_2\text{O}$  chemical analog of hummerite and pascoite. *Am. Mineral.* **1965**, *50*, 284–285.
34. Evans, H.T. Molecular structure of isopoly complex ion decavanadate ( $\text{V}_{10}\text{O}_{28}^{6-}$ ). *Inorg. Chem.* **1966**, *5*, 967–977. [[CrossRef](#)]
35. Evans, H.T.; Swallow, A.G.; Barnes, W.H. Structure of decavanadate ion. *J. Am. Chem. Soc.* **1964**, *86*, 4209–4210. [[CrossRef](#)]
36. Evans, H.T.; Mrose, M.E.; Marvin, R. Constitution of the natural and artificial decavanadates. *Geol. Soc. Am. Bull.* **1954**, *65*, 1249.
37. Evans, H.T.; Mrose, M.E. A crystal chemical study of Montroseite and Paramontroseite. *Am. Mineral.* **1955**, *40*, 861–875.
38. Gordillo, C.E.; Linares, E.; Toubes, R.O.; Winchell, H. Huemulite  $\text{Na}_4\text{MgV}_{10}\text{O}_{28}\cdot 24\text{H}_2\text{O}$  a new hydrous sodium and magnesium vanadate from Huemul Mine Mendoza Province, Argentina. *Am. Mineral.* **1966**, *51*, 1–13.
39. Evans, H.T.; Garrels, R.M. Thermodynamic equilibrii of vanadium in aqueous systems as applied to the interpretation of the Colorado Plateau ore deposits. *Geochim. Cosmochim. Acta.* **1959**, *15*, 131–149. [[CrossRef](#)]
40. Hansley, P.; Spirakis, C. The Pascoite Family of Minerals, Including the Redefinition of Rakovanite. *Econ. Geol.* **1992**, *87*, 352–365. [[CrossRef](#)]
41. Wanty, R.B.; Goldhaber, M.B. Thermodynamics and Kinetics of Reactions Involving Vanadium in Natural Systems—Accumulation of Vanadium in Sedimentary-Rocks. *Geochim. Cosmochim. Acta.* **1992**, *56*, 1471–1483. [[CrossRef](#)]
42. Evans, H.T.; Mrose, M.E. The crystal structures of 3 new vanadium oxide minerals. *Acta Crystallogr.* **1958**, *11*, 56–58. [[CrossRef](#)]

43. Palke, A.C.; Stebbins, J.F.; Boatner, L.A. P-31 Magic Angle Spinning NMR Study of Flux-Grown Rare-Earth Element Orthophosphate (Monazite/Xenotime) Solid Solutions: Evidence of Random Cation Distribution from Paramagnetically Shifted NMR Resonances. *Inorg. Chem.* **2013**, *52*, 12605–12615. [[CrossRef](#)]
44. Crans, D.C.; Peters, B.J.; Wu, X.; McLauchlan, C.C. Does anion-cation organization in Na<sup>+</sup>-containing X-ray crystal structures relate to solution interactions in inhomogeneous nanoscale environments: Sodium-decavanadate in solid state materials, minerals, and microemulsions. *Coord. Chem. Rev.* **2017**, *344*, 115–130. [[CrossRef](#)]
45. Hillebrand, W.F.; Merwin, H.E.; Wright, F.E. Hewettite, Metahewettite, and Pascoite, Hydrated Calcium Vanadates. *Am. Philos. Soc.* **1914**, *53*, 31–54.
46. Kampf, A.R.; Nash, B.P.; Adams, P.M.; Marty, J.; Hughes, J.M. Ammoniolasalite, (NH<sub>4</sub>)<sub>2</sub>Mg<sub>2</sub>(H<sub>2</sub>O)<sub>20</sub>V<sub>10</sub>O<sub>28</sub>, a new decavanadate species from the Burro Mine, Slick Rock District, Colorado. *Can. Mineral.* **2018**, *56*, 859–869. [[CrossRef](#)]
47. Kampf, A.R.; Hughes, J.M.; Marty, J.; Nash, B.P.; Chen, Y.S.; Steele, I.M. Bluestreakite, K<sub>4</sub>Mg<sub>2</sub>(V<sub>2</sub><sup>4+</sup>V<sub>8</sub><sup>5+</sup>O<sub>28</sub>)·14H<sub>2</sub>O, a new mixed-valence decavanadate mineral from the Blue Streak Mine, Montrose County, Colorado: Crystal structure and descriptive mineralogy. *Can. Mineral.* **2014**, *52*, 1007–1018. [[CrossRef](#)]
48. Kampf, A.R.; Nash, B.P.; Hughes, J.M.; Marty, J. Burroite, Ca<sub>2</sub>(NH<sub>4</sub>)<sub>2</sub>(V<sub>10</sub>O<sub>28</sub>)·15H<sub>2</sub>O, a new decavanadate mineral from the Burro Mine, San Miguel County, Colorado. *Can. Mineral.* **2017**, *55*, 473–481. [[CrossRef](#)]
49. Kampf, A.R.; Cooper, M.A.; Hughes, J.M.; Nash, B.P.; Hawthorne, F.C.; Marty, J. Caseyite, a new mineral containing a variant of the flat-Al-13 polyoxometalate cation. *Am. Mineral.* **2020**, *105*, 123–131. [[CrossRef](#)]
50. Kampf, A.R.; Hughes, J.M.; Marty, J.; Nash, B. Gunterite, Na<sub>4</sub>(H<sub>2</sub>O)<sub>16</sub>(H<sub>2</sub>V<sub>10</sub>O<sub>28</sub>)·6H<sub>2</sub>O, a new mineral species with a doubly-protonated decavanadate polyanion: Crystal structure and descriptive mineralogy. *Can. Mineral.* **2011**, *49*, 1243–1251. [[CrossRef](#)]
51. Kampf, A.R.; Cooper, M.A.; Hawthorne, F.C.; Hughes, J.M.; Nash, B.P.; Adams, P.M. The redefinition of Gunterite, Na<sub>4</sub>Ca V<sub>10</sub>O<sub>28</sub>·20H<sub>2</sub>O. *Can. Mineral.* **2022**, *60*, 361–368. [[CrossRef](#)]
52. Colombo, F.; Baggio, R.; Kampf, A.R. The crystal structure of the elusive Huemulite. *Can. Mineral.* **2011**, *49*, 849–864. [[CrossRef](#)]
53. Rakovan, J.; Schmidt, G.R.; Gunter, M.E.; Nash, B.; Marty, J.; Kampf, A.R.; Wise, W.S. Hughesite, Na<sub>3</sub>Al(V<sub>10</sub>O<sub>28</sub>)·22H<sub>2</sub>O, a new member of the Pascoite family of minerals from the Sunday Mine, San Miguel County, Colorado. *Can. Mineral.* **2011**, *49*, 1253–1265. [[CrossRef](#)]
54. Weeks, A.D.; Cisney, E.A.; Sherwood, A.M. Hummerite and montroseite, 2 vanadium minerals from Montrose County, Colorado. *Am. Mineral.* **1951**, *36*, 326–327.
55. Hughes, J.M.; Schindler, M.; Rakovan, J.; Cureton, F.E. The crystal structure of hummerite, KMg(V<sub>5</sub>O<sub>14</sub>)·8H<sub>2</sub>O: Bonding between the V<sub>10</sub>O<sub>28</sub><sup>6-</sup> structural unit and the {K<sub>2</sub>Mg<sub>2</sub>(H<sub>2</sub>O)<sub>16</sub>}<sup>6+</sup> interstitial complex. *Can. Mineral.* **2002**, *40*, 1429–1435. [[CrossRef](#)]
56. Kampf, A.R.; Nash, B.P.; Marty, J.; Hughes, J.M.; Rose, T.P. Hydropascoite, Ca<sub>3</sub>(V<sub>10</sub>O<sub>28</sub>)·24H<sub>2</sub>O, a new decavanadate mineral from the Packrat Mine, Mesa County, Colorado. *Can. Mineral.* **2017**, *55*, 207–217. [[CrossRef](#)]
57. Kampf, A.R.; Hughes, J.M.; Nash, B.P.; Marty, J.; Cooper, M.A.; Hawthorne, F.C.; Karpenko, V.Y.; Pautov, L.A.; Agakhanov, A.A. Revision of the formula of Wernerbaurite and Schindlerite: Ammonium rather than hydronium-bearing decavanadate minerals. *Can. Mineral.* **2016**, *54*, 555–558. [[CrossRef](#)]
58. Hughes, J.M.; Wise, W.S.; Gunter, M.E.; Morton, J.P.; Rakovan, J. Lasalite, Na<sub>2</sub>Mg<sub>2</sub>V<sub>10</sub>O<sub>28</sub>·20H<sub>2</sub>O, a new decavanadate mineral species from the Vanadium Queen Mine, La Sal District, Utah: Description, atomic arrangement, and relationship to the Pascoite group of minerals. *Can. Mineral.* **2008**, *46*, 1365–1372. [[CrossRef](#)]
59. Kampf, A.R.; Steele, I.M. Magnesiopascoite, a new member of the Pascoite group: Description and crystal structure. *Can. Mineral.* **2008**, *43*, 679–686. [[CrossRef](#)]
60. Kampf, A.R.; Hughes, J.M.; Marty, J.; Brown, F.H. Nashite, Na<sub>3</sub>Ca<sub>2</sub>(V<sup>4+</sup>V<sup>5+</sup>)O<sub>28</sub>·24H<sub>2</sub>O, a new mineral species from the Yellow Cat Mining District, Utah and the Slick Rock Mining District, Colorado: Crystal structure and descriptive mineralogy. *Can. Mineral.* **2013**, *51*, 27–37. [[CrossRef](#)]
61. Hughes, J.M.; Schindler, M.; Francis, C.A. The C2/m disordered structure of pascoite, Ca<sub>3</sub>V<sub>10</sub>O<sub>28</sub>·17H<sub>2</sub>O: Bonding between structural units and interstitial complexes in compounds containing the V<sub>10</sub>O<sub>28</sub><sup>6-</sup> decavanadate polyanion. *Can. Mineral.* **2005**, *43*, 1379–1386. [[CrossRef](#)]
62. Kampf, A.R.; Hughes, J.M.; Marty, J.; Nash, B. Postite, Mg(H<sub>2</sub>O)<sub>6</sub>Al<sub>2</sub>(OH)<sub>2</sub>(H<sub>2</sub>O)<sub>8</sub>(V<sub>10</sub>O<sub>28</sub>)·13H<sub>2</sub>O, a new mineral species from the La Sal Mining District, Utah: Crystal structure and descriptive mineralogy. *Can. Mineral.* **2012**, *50*, 45–53. [[CrossRef](#)]
63. Kampf, A.R.; Cooper, M.A.; Hughes, J.M.; Ma, C.; Casey, W.H.; Hawthorne, F.C.; Marty, J. Protocaseyite, a new decavanadate mineral containing a Al<sub>4</sub>(OH)<sub>6</sub>(H<sub>2</sub>O)<sub>12</sub><sup>6+</sup> linear tetramer, a novel isopolycation. *Am. Mineral.* **2022**, *107*, 1181–1189. [[CrossRef](#)]
64. Kampf, A.R.; Hughes, J.M.; Marty, J.; Gunter, M.E.; Nash, B. Rakovanite, Na<sub>3</sub>{H<sub>3</sub>V<sub>10</sub>O<sub>28</sub>}·15H<sub>2</sub>O, a new member of the Pascoite family with a protonated decavanadate polyanion. *Can. Mineral.* **2011**, *49*, 595–604. [[CrossRef](#)]
65. Kampf, A.R.; Hughes, J.M.; Marty, J.; Nash, B. Wernerbaurite, {[Ca(H<sub>2</sub>O)<sub>7</sub>]<sub>2</sub>(H<sub>2</sub>O)<sub>2</sub>(H<sub>3</sub>O)<sub>2</sub>}{V<sub>10</sub>O<sub>28</sub>}, and Schindlerite {[Na<sub>2</sub>(H<sub>2</sub>O)<sub>10</sub>](H<sub>3</sub>O)<sub>4</sub>}{V<sub>10</sub>O<sub>28</sub>}, the first hydronium-bearing decavanadate minerals. *Can. Mineral.* **2013**, *51*, 297–312. [[CrossRef](#)]
66. Olds, T.A.; Kampf, A.R.; Cooper, M.A.; Adams, P.M.; Marty, J. Trebiskyite, IMA 2019-131. CNMNC Newsletter. *Mineral. Mag.* **2020**, *84*, 485–488. [[CrossRef](#)]
67. Warr, L.N. IMA-CNMNC approved mineral symbols. *Mineral. Mag.* **2021**, *85*, 291–320. [[CrossRef](#)]
68. Strunz, H.N.; Nickel, E.H. *Strunz Mineralogical Tables: Chemical Structural Mineral Classification System*, 9th ed.; Schweizerbart: Stuttgart, Germany, 2001.
69. Hawthorne, F.C. Graphical enumeration of polyhedral clusters. *Acta Crystallogr. A* **1983**, *39*, 724–736. [[CrossRef](#)]

70. Hawthorne, F.C.; Hughes, J.M.; Cooper, M.A.; Kampf, A.R. Bonding between the decavanadate polyanion and the interstitial complex in Pascoite-family minerals. *Can. Mineral.* **2022**, *60*, 341–359. [[CrossRef](#)]
71. Schindler, M.; Hawthorne, F.C.; Baur, W.H. A crystal-chemical approach to the composition and occurrence of vanadium minerals. *Can. Mineral.* **2000**, *38*, 1443–1456. [[CrossRef](#)]
72. Schindler, M.; Hawthorne, F.C. A bond-valence approach to the structure, chemistry and paragenesis of hydroxy-hydrated oxysalt minerals. I. Theory. *Can. Mineral.* **2001**, *39*, 1225–1242. [[CrossRef](#)]
73. Hawthorne, F.C. The role of OH and H<sub>2</sub>O in oxide and oxysalt minerals. *Z. Kristallogr.* **1992**, *201*, 183–206. [[CrossRef](#)]
74. Schindler, M.; Hawthorne, F.C.; Baur, W.H. Crystal chemical aspects of vanadium: Polyhedral geometries, characteristic bond valences, and polymerization of (VOn) polyhedra. *Chem. Mater.* **2000**, *12*, 1248–1259. [[CrossRef](#)]
75. da Silva, J.L.F.; da Piedade, M.F.M.; Duarte, M.T. Decavanadates: A building-block for supramolecular assemblies. *Inorg. Chim. Acta.* **2003**, *356*, 222–242. [[CrossRef](#)]
76. Bosnjakovic-Pavlovic, N.; Prevost, J.; de Bire Spasojevic, A. Crystallographic Statistical Study of Decavanadate Anion Based-Structures: Toward a Prediction of Noncovalent Interactions. *Crys. Growth Des.* **2011**, *11*, 3778–3789. [[CrossRef](#)]
77. Nakamura, S.; Ozeki, T. Hydrogen-bonded aggregates of protonated decavanadate anions in their tetraalkylammonium salts. *J. Chem. Soc. Dalton. Trans.* **2001**, *4*, 472–480. [[CrossRef](#)]
78. Bindi, L.; Nespolo, M.; Krivovichev, S.V.; Chapuis, G.; Biagioni, C. Producing highly complicated materials. Nature does it better. *Rep. Prog. Phys.* **2020**, *83*, 106501. [[CrossRef](#)]
79. Phillips, B.L. *Crystallography and NMR: Applications to Geochemistry*; John Wiley & Sons, Ltd.: Hoboken, NJ, USA, 2009.
80. Burns, P.C. Complex minerals preserve natural geochemically important nanoscale metal oxide clusters. *Acta Crystallogr. B Struct. Sci. Cryst. Eng. Mater.* **2020**, *76*, 512–513. [[CrossRef](#)]
81. Stebbins, J.F.; Xue, X.Y. NMR Spectroscopy of Inorganic Earth Materials. In *Spectroscopic Methods in Mineralogy and Materials Sciences*; Reviews in Mineralogy & Geochemistry; Henderson, G.S., Neuville, D.R., Downs, R.T., Eds.; Mineralogical Society of America: Chantilly, VA, USA, 2014; Volume 78, pp. 605–653.
82. Huang, W.; Todaro, L.; Francesconi, L.C.; Polenova, T. <sup>51</sup>V Magic Angle Spinning NMR Spectroscopy of Six-Coordinate Lindqvist Oxoanions: A Sensitive Probe for the Electronic Environment in Vanadium-Containing Polyoxometalates. Counterions Dictate the <sup>51</sup>V Fine Structure Constants in Polyoxometalate Solids. *J. Am. Chem. Soc.* **2003**, *125*, 5928–5938. [[CrossRef](#)]
83. Huang, W.; Todaro, L.; Yap, G.P.A.; Beer, R.; Francesconi, L.C.; Polenova, T. <sup>51</sup>V Magic Angle Spinning NMR Spectroscopy of Keggin Anions [PV<sub>n</sub>W<sub>12-n</sub>O<sub>40</sub>]<sup>(3+n)-</sup>: Effect of Counteraction and Vanadium Substitution on Fine Structure Constants. *J. Am. Chem. Soc.* **2004**, *126*, 11564–11573. [[CrossRef](#)]
84. Lapina, O.B.; Khabibulin, D.F.; Shubin, A.A.; Tersikh, V.V. Practical aspects of V-51 and Nb-93 solid-state NMR spectroscopy and applications to oxide materials. *Prog. Nucl. Magn. Reson. Spectrosc.* **2008**, *53*, 128–191. [[CrossRef](#)]
85. Nielsen, U.G.; Jakobsen, H.J.; Skibsted, J. Characterization of Divalent Metal Metavanadates by <sup>51</sup>V Magic-Angle Spinning NMR Spectroscopy of the Central and Satellite Transitions. *Inorg. Chem.* **2000**, *39*, 2135–2145. [[CrossRef](#)] [[PubMed](#)]
86. Pooransingh, N.; Pomerantseva, E.; Ebel, M.; Jantzen, S.; Rehder, D.; Polenova, T. <sup>51</sup>V Solid-State Magic Angle Spinning NMR Spectroscopy and DFT Studies of Oxovanadium(V) Complexes Mimicking the Active Site of Vanadium Haloperoxidases. *Inorg. Chem.* **2003**, *42*, 1256–1266. [[CrossRef](#)] [[PubMed](#)]
87. Rehder, D.; Polenova, T.; Bühl, M. Vanadium-51 NMR. *Annu. Rep. NMR Spectrosc.* **2007**, *62*, 50–114.
88. Skibsted, J.; Jacobsen, C.J.H.; Jacobsen, H.J. <sup>51</sup>V Chemical Shielding and Quadrupole Coupling in Ortho- and Metavanadates from <sup>51</sup>V MAS NMR Spectroscopy. *Inorg. Chem.* **1998**, *37*, 3083–3092. [[CrossRef](#)]
89. Shubin, A.A.; Lapina, O.B.; Bondareva, V.M. Characterisation of strongly bonded V(V) species in VOx/TiO<sub>2</sub> catalyst by static and MAS solid-state V-51 NMR spectroscopy. *Chem. Phys. Lett.* **1999**, *302*, 341–346. [[CrossRef](#)]
90. Crans, D.C.; Levinger, N.E. The Conundrum of pH in Water Nanodroplets: Sensing pH in Reverse Micelle Water Pools. *Acc. Chem. Res.* **2012**, *45*, 1637–1645. [[CrossRef](#)]
91. Ronconi, L.; Sadler, P.J. Applications of heteronuclear NMR spectroscopy in biological and medicinal inorganic chemistry. *Coord. Chem. Rev.* **2008**, *252*, 2239–2277. [[CrossRef](#)]
92. Howarth, O.W. Vanadium-51 NMR. *Prog. Nucl. Magn. Reson. Spectrosc.* **1990**, *22*, 453–485. [[CrossRef](#)]
93. Harris, R.K. *NMR and the Periodic Table*; Academic Press: Cambridge, MA, USA, 1978.
94. Templeton, D.M.; Ariese, F.; Cornelis, R.; Danielsson, L.G.; Muntau, H.; Van Leeuwen, H.P.; Lobinski, R. Guidelines for terms related to chemical speciation and fractionation of elements. Definitions, structural aspects, and methodological approaches (IUPAC Recommendations 2000). *Pure Appl. Chem.* **2000**, *72*, 1453–1470. [[CrossRef](#)]
95. Szpunar, J. Bio-inorganic speciation analysis by hyphenated techniques. *Analyst* **2000**, *125*, 936–988. [[CrossRef](#)]
96. Szpunar, J. Advances in analytical methodology for bioinorganic speciation analysis: Metallomics, metalloproteomics and heteroatom-tagged proteomics and metabolomics. *Analyst* **2005**, *130*, 442–465. [[CrossRef](#)]
97. Lobinski, R.; Becker, J.S.; Haraguchi, H.; Sarkar, B. Metallomics: Guidelines for terminology and critical evaluation of analytical chemistry approaches (IUPAC Technical Report). *Pure Appl. Chem.* **2010**, *82*, 493–504. [[CrossRef](#)]
98. Markham, S.A.; Crans, D.C.; Atwater, B.A. Using speciation to gain insight into sustainable coupling reactions and their catalysts. In *Catalysis for a Sustainable Environment*; Crans, D.C., Bruce, A., Atwater, B.A., Eds.; Wiley: Hoboken, NJ, USA, 2022; *in press*.
99. Kiss, T.; Buglyo, P.; Sanna, D.; Micera, G.; Decock, P.; Dewaele, D. Oxovanadium(IV) complexes of citric and tartaric acids in aqueous solution. *Inorg. Chim. Acta* **1995**, *239*, 145–153. [[CrossRef](#)]

100. Baes, C.F.; Mesmer, R.E. *The Hydrolysis of Cations*; John Wiley & Sons: New York, NY, USA, 1976; p. 254.
101. Timerbaev, A.R. Element Speciation Analysis Using Capillary Electrophoresis: Twenty Years of Development and Applications. *Chem. Rev.* **2013**, *113*, 778–812. [[CrossRef](#)]
102. Crans, D.C.; Ehde, P.M.; Shin, P.K.; Pettersson, L. Structural and kinetic characterization of simple complexes as models for vanadate protein interactions. *J. Am. Chem. Soc.* **1991**, *113*, 3728–3736. [[CrossRef](#)]
103. Crans, D.C.; Woll, K.A.; Prusinskas, K.; Johnson, M.D.; Norkus, E. Metal Speciation in Health and Medicine Represented by Iron and Vanadium. *Inorg. Chem.* **2013**, *52*, 12262–12275. [[CrossRef](#)]
104. Crans, D.C.; Smee, J.J.; Gaidamauskas, E.; Yang, L.Q. The chemistry and biochemistry of vanadium and the biological activities exerted by vanadium compounds. *Chem. Rev.* **2004**, *104*, 849–902. [[CrossRef](#)]
105. Baruah, B.; Roden, J.M.; Sedgwick, M.; Correa, N.M.; Crans, D.C.; Levinger, N.E. When is water not water? Exploring water confined in large reverse micelles using a highly charged inorganic molecular probe. *J. Am. Chem. Soc.* **2006**, *128*, 12758–12765. [[CrossRef](#)]
106. Bak, M.; Rasmussen, J.T.; Nielsen, N.C. SIMPSON: A general simulation program for solid-state NMR spectroscopy. *J. Mag. Res.* **2000**, *147*, 296–330. [[CrossRef](#)]
107. Frisch, M.J.T.G.W.; Schlegel, H.B.; Scuseria, G.E.; Robb, M.A.; Cheeseman, J.R.; Montgomery, J.A., Jr.; Vreven, T.; Kudin, K.N.; Burant, J.C.; Millam, J.M.; et al. *Gaussian 03, Revision C.02*; Gaussian, Inc.: Wallingford, CT, USA, 2004.
108. Nielsen, U.G.; Jakobsen, H.J.; Skibsted, J. 51V MAS NMR Investigation of 51V Quadrupole Coupling and Chemical Shift Anisotropy in Divalent Metal Pyrovanadates. *J. Phys. Chem. B* **2001**, *105*, 420–429. [[CrossRef](#)]
109. Crans, D.C.; Felty, R.A.; Chen, H.; Eckert, H.; Das, N. Oxovanadium(V) Alkoxide Derivatives of 1,2-Diols: Synthesis and Solid-State <sup>51</sup>V NMR Characterization. *Inorg. Chem.* **1994**, *33*, 2427–2438. [[CrossRef](#)]
110. Eckert, H.; Wachs, I.E. Solid-state vanadium-51 NMR structural studies on supported vanadium(V) oxide catalysts: Vanadium oxide surface layers on alumina and titania supports. *J. Phys. Chem.* **1989**, *93*, 6796–6805. [[CrossRef](#)]
111. Hayakawa, S.; Yoko, T.; Sakka, S. <sup>51</sup>V NMR Studies of Crystalline Divalent Metal Vanadates and Divanadates. *Bull. Chem. Soc. Jpn.* **1993**, *66*, 3393. [[CrossRef](#)]
112. Hayakawa, S.; Yoko, T.; Sakka, S. <sup>51</sup>V NMR studies of crystalline monovalent and divalent metal metavanadates. *J. Solid State Chem.* **1994**, *112*, 329–339. [[CrossRef](#)]
113. Harris, R.K.; Becker, E.D.; Cabral de Menezes, S.M.; Goodfellow, R.; Granger, P. NMR nomenclature. Nuclear spin properties and conventions for chemical shifts (IUPAC Recommendations 2001). *Pure Appl. Chem.* **2001**, *73*, 1795–1818. [[CrossRef](#)]
114. Mackenzie, K.J.D.; Smith, M.E. *Multinuclear Solid-State NMR of Inorganic Materials*; Pergamon: Oxford, UK, 2002.
115. Pooransingh-Margolis, N.; Renirie, R.; Hasan, Z.; Wever, R.; Vega, A.J.; Polenova, T. <sup>51</sup>V Solid-State Magic Angle Spinning NMR Spectroscopy of Vanadium Chloroperoxidase. *J. Am. Chem. Soc.* **2006**, *128*, 5190–5208. [[CrossRef](#)]
116. Buhl, M.; Hamprecht, F.A. Theoretical investigations of NMR chemical shifts and reactivities of oxovanadium(V) compounds. *J. Comput. Chem.* **1998**, *19*, 113–122. [[CrossRef](#)]
117. Ooms, K.J.; Wasylshen, R.E. Solid-State Ru-99 NMR Spectroscopy: A Useful Tool for Characterizing Prototypal Diamagnetic Ruthenium Compounds. *J. Am. Chem. Soc.* **2004**, *126*, 10972–10980. [[CrossRef](#)]
118. Bühl, M.; Parrinello, M. Medium Effects on <sup>51</sup>V NMR Chemical Shifts: A Density Functional Study. *Chem. Eur. J.* **2001**, *7*, 4487–4494. [[CrossRef](#)]
119. Gee, B.A. Vanadium-51 solid state NMR electric field gradient tensors: A DFT embedded ion and isolated cluster study of crystalline vanadium oxides. *Solid State Nucl. Mag. Reson.* **2006**, *30*, 171–181. [[CrossRef](#)]
120. Feindel, K.W.; Ooms, K.J.; Wasylshen, R.E. A solid-state <sup>55</sup>Mn NMR spectroscopy and DFT investigation of manganese pentacarbonyl compounds. *Phys. Chem. Chem. Phys.* **2007**, *9*, 1226–1238. [[CrossRef](#)]
121. Palke, A.C.; Stebbins, J.F. Paramagnetic interactions in the P-31 NMR spectroscopy of rare earth element orthophosphate (REPO<sub>4</sub>, monazite/xenotime) solid solutions. *Am. Mineral.* **2011**, *96*, 1343–1353. [[CrossRef](#)]
122. Bertini, I.; Luchinat, C.; Parigi, G. Magnetic susceptibility in paramagnetic NMR. *Prog. Nucl. Mag. Res. Spec.* **2002**, *40*, 249–273. [[CrossRef](#)]
123. Pell, A.J.; Pintacua, G.; Grey, C.P. Paramagnetic NMR in solution and the solid state. *Prog. Nucl. Magn. Reson. Spectrosc.* **2019**, *111*, 1–271. [[CrossRef](#)]
124. Bosi, F.; Reznitskii, L.; Skogby, H.; Halenius, U. Vanadio-oxy-chromium-dravite, NaV<sub>3</sub>(Cr<sub>4</sub>Mg<sub>2</sub>)(Si<sub>6</sub>O<sub>18</sub>)(BO<sub>3</sub>)<sub>3</sub>(OH)<sub>3</sub>O a new mineral species of the tourmaline supergroup. *Am. Mineral.* **2014**, *99*, 1155–1162. [[CrossRef](#)]
125. Bosi, F.; Reznitskii, L.Z.; Sklyarov, E.V. Oxy-vanadium-dravite, NaV<sub>3</sub>(V<sub>4</sub>Mg<sub>2</sub>)(Si<sub>6</sub>O<sub>18</sub>)(BO<sub>3</sub>)<sub>3</sub>(OH)<sub>3</sub>O: Crystal structure and redefinition of the “vanadium-dravite” tourmaline. *Am. Mineral.* **2013**, *98*, 501–505. [[CrossRef](#)]
126. Bosi, F.; Skogby, H.; Reznitskii, L.; Halenius, U. Vanadio-oxy-dravite, NaV<sub>3</sub>(Al<sub>4</sub>Mg<sub>2</sub>)(Si<sub>6</sub>O<sub>18</sub>)(BO<sub>3</sub>)<sub>3</sub>(OH)<sub>3</sub>O, a new mineral species of the tourmaline supergroup. *Am. Mineral.* **2014**, *99*, 218–224. [[CrossRef](#)]
127. Das, N.; Eckert, H.; Hu, H.C.; Wachs, I.E.; Walzer, J.F.; Feher, F.J. Bonding states of surface vanadium(V) oxide phases on silica—Structural characterization by <sup>51</sup>V NMR and Raman spectroscopy. *J. Phys. Chem.* **1993**, *97*, 8240–8243. [[CrossRef](#)]
128. Jaegers, N.R.; Wan, C.; Hu, M.Y.; Vasiliu, M.; Dixon, D.A.; Walter, E.; Wachs, I.E.; Wang, Y.; Hu, J.Z. Investigation of Silica-Supported Vanadium Oxide Catalysts by High Field V-51 Magic-Angle Spinning NMR. *J. Phys. Chem. C* **2017**, *121*, 6246–6254. [[CrossRef](#)]

129. Zeman, O.E.O.; Hochleitner, R.; Schmahl, W.W.; Karaghiosoff, K.; Brauniger, T. Relationship between Pb-207 NMR chemical shift and the morphology and crystal structure for the apatites  $Pb_5(AO_4)_3Cl$ , vanadinite ( $A = V$ ), pyromorphite ( $A = P$ ), and mimetite ( $A = As$ ). *Am. Mineral.* **2021**, *106*, 541–548. [[CrossRef](#)]
130. Li, C.Y.; Hsieh, C.Y.; Lin, H.M.; Kao, H.M.; Lii, K.H. High-temperature, high-pressure hydrothermal synthesis, crystal structure, and solid state NMR spectroscopy of a new Vanadium(IV) silicate:  $Rb_2(VO)(Si_4O_{10}) \cdot xH_2O$ . *Inorg. Chem.* **2002**, *41*, 4206–4210. [[CrossRef](#)] [[PubMed](#)]
131. Quillam, J.A.; Bert, F.; Colman, R.H.; Boldrin, D.; Wills, A.S.; Mendels, P. Ground state and intrinsic susceptibility of the kagome antiferromagnet vesignieite as seen by  $^{51}V$  NMR. *Phys. Rev. B* **2011**, *84*, 180401. [[CrossRef](#)]
132. Yoshida, M.; Okamoto, Y.; Takigawa, M.; Hiroi, Z. Magnetic Order in the Spin-1/2 Kagome Antiferromagnet Vesignieite. *J. Phys. Soc. Jpn.* **2013**, *82*, 013702. [[CrossRef](#)]
133. Pozarnsky, G.A.; McCormick, A.V. V-51 NMR and EPR study of reaction-kinetics and mechanisms in  $V_2O_5$  gelation by ion-exchange of sodium metavanadate solutions. *Chem. Mater.* **1994**, *6*, 380–385. [[CrossRef](#)]
134. Favre, D.; Bobst, C.E.; Eyles, S.J.; Murakami, H.; Crans, D.C.; Kaltashov, I.A. Solution- and gas-phase behavior of decavanadate: Implications for mass spectrometric analysis of redox-active polyoxidometalates. *Inorg. Chem. Front.* **2022**, *9*, 1556–1564. [[CrossRef](#)] [[PubMed](#)]
135. Althumairy, D.; Postal, K.; Barisas, B.G.; Nunes, G.G.; Roess, D.A.; Crans, D.C. Polyoxometalates Function as Indirect Activators of a G Protein-Coupled Receptor. *Metallomics* **2020**, *12*, 1044–1061. [[CrossRef](#)]